Triboelectric Nanogenerator Enabled Body Sensor Network for Self-Powered Human Heart-Rate Monitoring

Zhiming **Lin**, [†] Jun **Chen**, [‡] Xiaoshi **Li**, [†] Zhihao **Zhou**, [†] Keyu **Meng**, [†] Wei **Wei**, [†] Jin **Yang**,*,[†] **and** Zhong Lin **Wang***, [‡, §]

[†] Department of Optoelectronic Engineering, Chongqing University, Chongqing 400044, China

[‡]School of Materials Science and Engineering, Georgia Institute of Technology, Atlanta, Georgia 30332, United States

[§]Beijing Institute of Nanoenergy and Nanosystems, Chinese Academy of Sciences, Beijing 100083, China

* Electronic mail: yangjin@cqu.edu.cn .

* zhong.wang@mse.gatech.edu .

KEYWORDS: self-powered body sensor network, triboelectric nanogenerator, downy structure, power management circuit, heart-rate monitoring

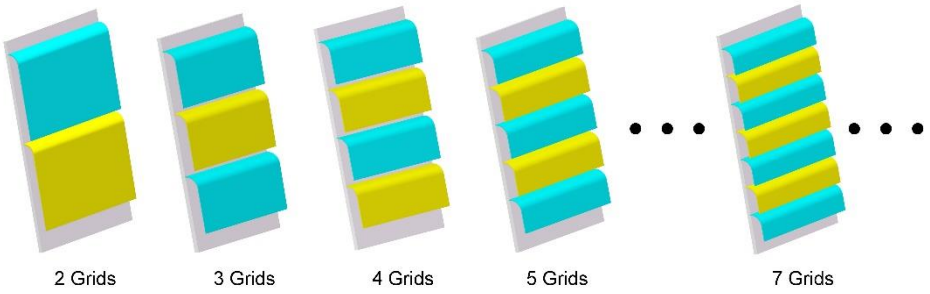

Figure S1. Schematic illustration of the inner downy structure with various grid numbers in a D-TENG.

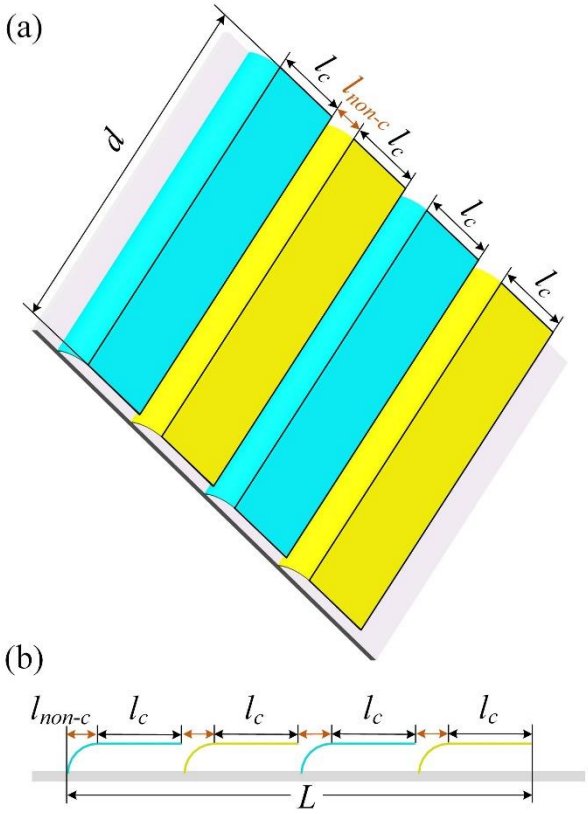

Figure S2. Illustration of the efficient triboelectric area of the inner downy structure.

Note 1: It can be observed that the efficient triboelectric area *S* can be expressed as

$$S = n \cdot l_c \cdot d \tag{1}$$

Here, n is the number of the inner downy structure, l_c is the length of contact area, and d is the width of the inner downy structure. Figure S2 (b) shows the section view of the inner downy structure, indicates that the length L can be predicted by

$$L = n(l_c + l_{non-c}) \tag{2}$$

Because all the types of D-TENGs share a same device volume, d and L are the constant values. Substituting Equation (1) into Equation (2) gives Equation (3) as

$$\mathrm{S} = n \cdot \left(\frac{L}{n} - l_{non-c}\right) d = L - ndl_{non-c} \tag{3}$$

It can be seen that the effective contact area will decrease with increasing of the grid numbers.

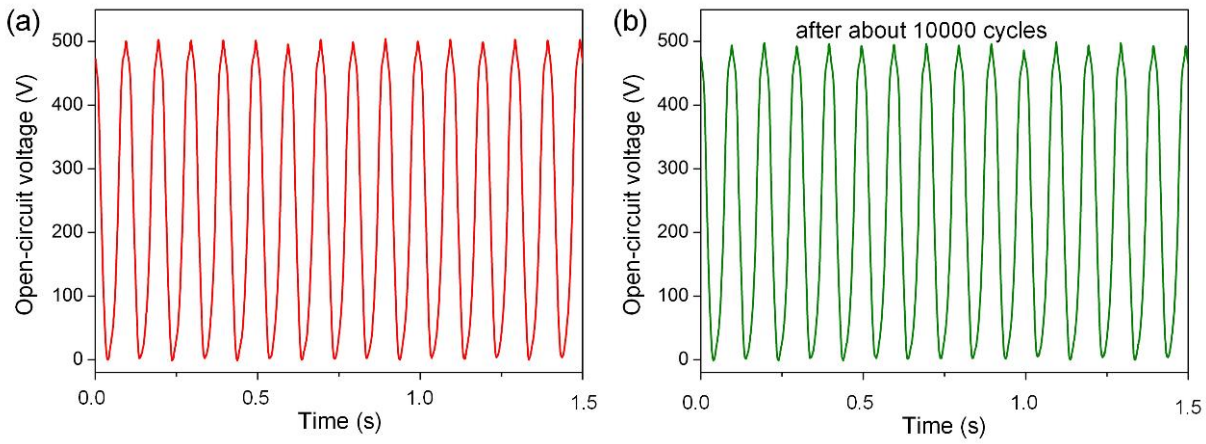

Figure S3. Cyclic test investigating the stability of the D-TENG. The measured open-circuit voltage of the D-TENG (a) before and (b) after about 10000 cycles.

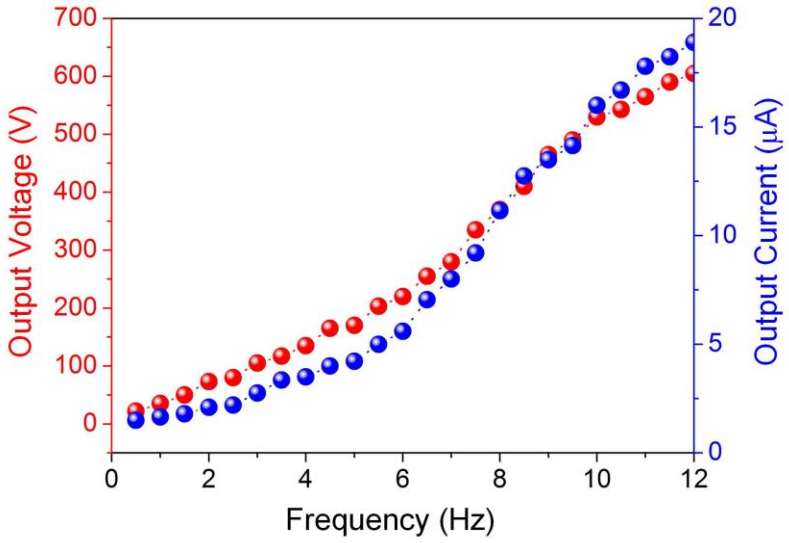

Figure S4. Relationship between frequency and electrical output of as-fabricated D-TENG with four grids at bands from 0.5 Hz to 12 Hz.

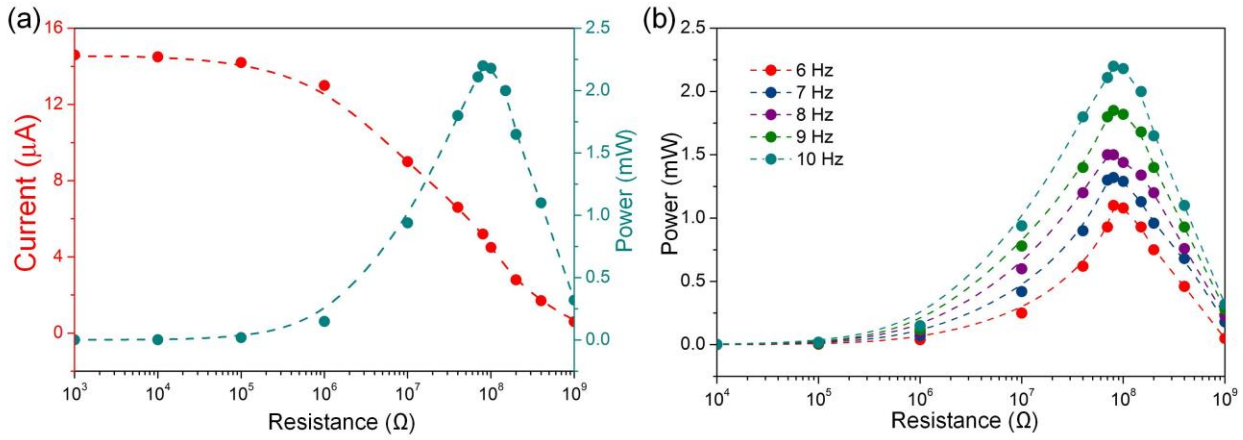

Figure S5. (a) The measured the output power of the D-TENG with four grids versus external load resistance. (b) The output power of D-TENGs with four grids at different frequencies versus external resistance.

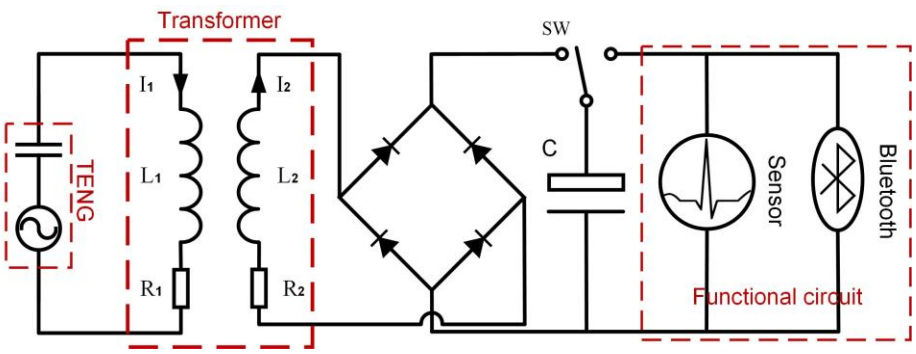

Figure S6. Diagram of the power management circuit.

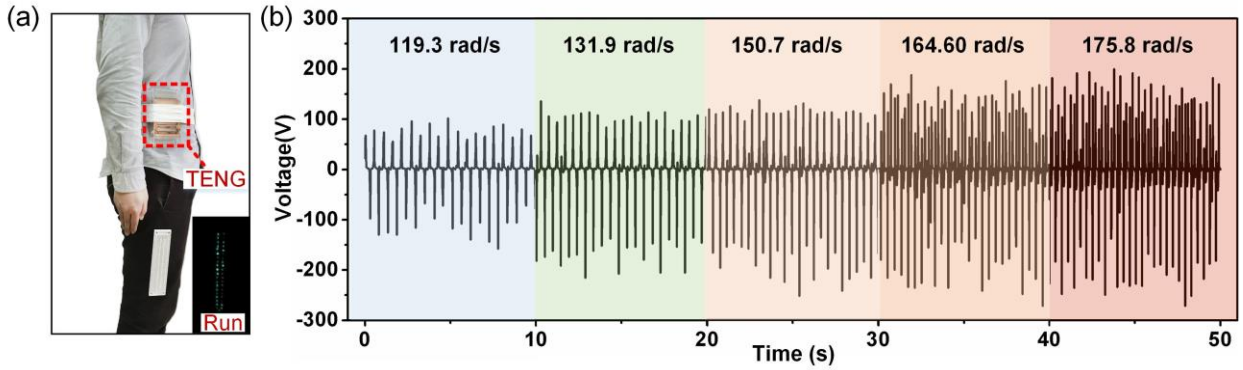

Figure S7. (a) Harvesting energy from natural vibration of human walking. (b) The open-circuit voltages of D-TENG at different frequencies of arm swinging.

Note 2: For the electrical output performance of the D-TENG, the theoretical model of metal-to-dielectric sliding mode is shown in Figure S8.

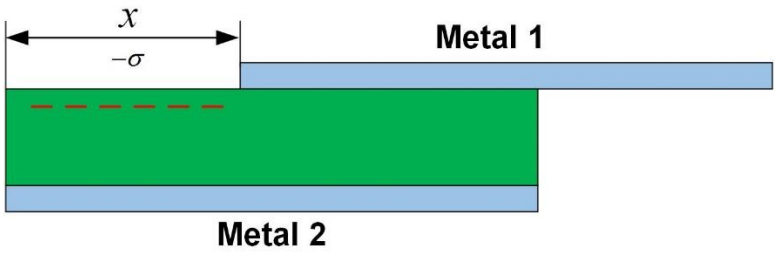

Figure S8. Theoretical model of metal-to-dielectric sliding mode.

In this mode, the bottom part is fixed while the top can slide through the longitudinal direction. And the lateral separation distance is defined as x. σ is the static charges with equal density of the inner surface of the two triboelectric layers due to contact electrification. And the amount of transferred charges between the two electrodes is defined as Q, then the V–Q–x relationship for the sliding mode TENGs by neglecting the edge effect can be expressed as [27]

$$V = -\frac{d_0}{W\varepsilon_0(l-x)}Q + \frac{\sigma d_0 x}{\varepsilon_0(l-x)} \tag{4}$$

where d_0 is the effective dielectric thickness, and ε_0 is the dielectric constant of a vacuum. W is the width of the two triboelectric layers. And Equation (4) can be rewritten as

$$V = \frac{d_0}{\varepsilon_0(l-x)}(x\sigma - \frac{Q}{W}) \tag{5}$$

It can be found that the output voltage will increase with the increasing separation distance x. the x can be calculated as

$$x = v_0 + at \tag{6}$$

where v_0 is the initial velocity of the sliding layer, and a is the acceleration of the sliding layer.

In the present research, a mechanical spring mass-damper model can be applied to analyze the motion characteristics of the harvester, as shown in Figure S9, and the governing equation of the harvester can be expressed as

$$\ddot{x} + 2\xi\omega_0\dot{x} + \omega_0^2 x = B\omega^2 e^{i\omega t} \tag{7}$$

where $\dot{x}$ and $\ddot{x}$ are the relative velocity and acceleration of the sliding layer with respect to the frame. ω_0 is the natural frequency of TENG, ω is the excitation frequency, $\xi = c/2\sqrt{km}$ is damping ratio, B is the input acceleration amplitude.

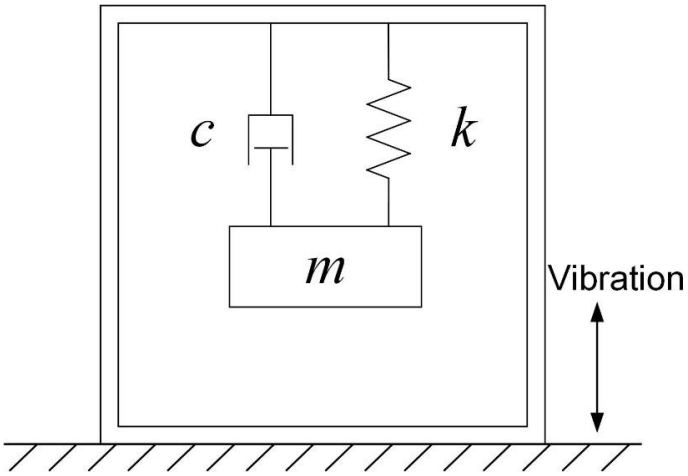

Figure S9. Mechanical spring mass-damper model.

Therefore, the lateral separation distance x can be calculated as

$$x = \beta B e^{i(\omega t - \theta)} \tag{8}$$

where $\beta(s) = s^2/\sqrt{(1-s^2)^2 + (2\xi s)^2}$,($s = \omega/\omega_0$), $\theta = \tanh^{-1}(2\xi s/1 - s^2)$. And then the acceleration of the sliding layer $\ddot{x}$ can be written as

$$\ddot{x} = -\beta B \omega^2 e^{i(\omega t - \theta)} \tag{9}$$

It can be observed that the acceleration $\ddot{x}$ is determined by parameter of the excitation frequency ω and input acceleration B. it is note that the acceleration $\ddot{x}$ is the acceleration of the sliding layer a in Equation (9).

Thus, according to the Equation (5), (6) and (9), the output voltage of TENG V is affect by the acceleration of the sliding layer a, which is determined by the excitation frequency ω and

input amplitude *B*, that is, the output performance of TENG is affected by the amplitude of human walking and the frequency of arm swinging. Figure S7 shows the electric output varies with different frequencies of arm swinging under a consistent amplitude. It can be observed that the open-circuit voltages presents an obvious increasing tendency with the increase of frequencies of arm swinging.

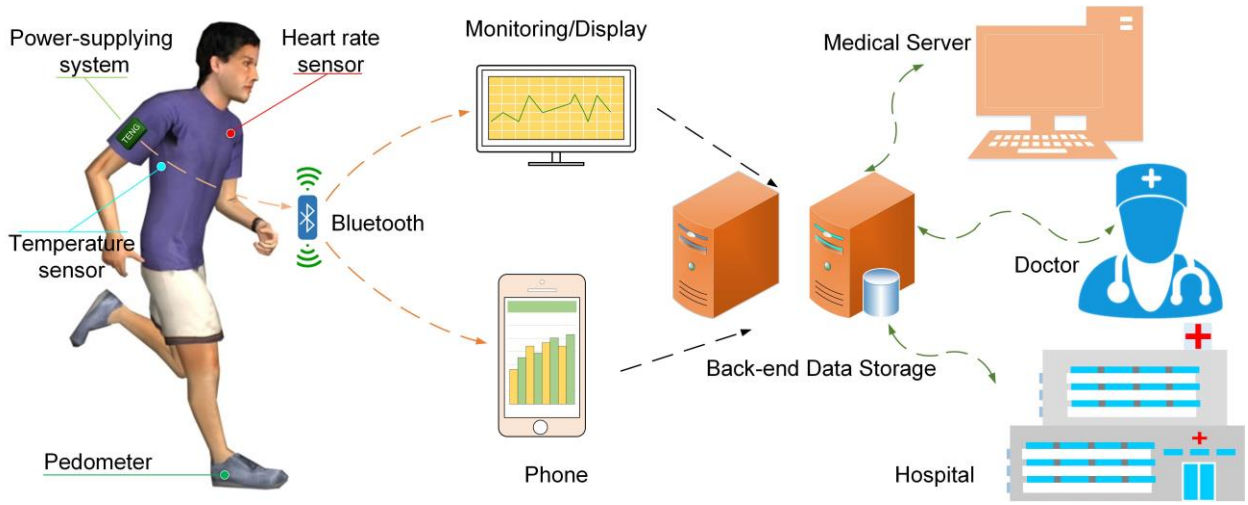

Figure S10. Schematic illustration of self-powered wireless body sensor network based on the power-supplying system for healthcare monitoring.